Controlled Release

Deutsche Ausgabe: DOI: 10.1002/ange.201607982
Internationale Ausgabe: DOI: 10.1002/anie.201607982

Block Copolymer Capsules with Structure-Dependent Release Behavior

Jiangping Xu[+], Jun Li[+], Yi Yang, Ke Wang, Nan Xu, Jingyi Li, Ruijing Liang, Lei Shen, Xiaolin Xie, Juan Tao, and Jintao Zhu**

Abstract: *Although high-boiling non-solvent induced macrophase separation in emulsion droplets has been widely applied for the fabrication of polymeric capsules, precise control of their structures remains a great challenge. Herein, block copolymer capsules with tunable shell structures were fabricated by employing a non-solvent as a liquid template in emulsion droplets. The properties of the non-solvents dictate the phase separation sequence in the droplets and the capsule formation mechanism. Two different pathways for capsule formation were observed, and could be applied to predict the shell structure. The structured capsules could be transformed into mesoporous capsules, which demonstrated an intriguing structure-dependent release behavior. Capsules with spherical shell structures displayed the best permeability, while those with lamellar shell structures showed the slowest release, but with a stepwise profile. After loading with an anticancer drug, different capsules induced different apoptosis ratios in cancer cell studies.*

Polymeric capsules are of great importance to many applications, especially for protecting loaded cargoes against a harsh environment and releasing them upon exposure to external triggers.[1–4] Many approaches,[5–7] such as phase separation in emulsion droplets,[8–10] sacrificial template guided polymerization,[11,12] layer-by-layer assembly techniques,[13–15] self-assembly of block copolymers (BCPs) in selective solvents,[16–20] and others, have been introduced for preparing polymeric capsules. Among these methods, the macrophase separation of a high-boiling non-solvent (HBNS, e.g., long-chain alkanes) in emulsion droplets containing a low-boiling good solvent (LBGS, e.g., chloroform) and a homopolymer has been developed as a simple yet versatile strategy for obtaining homopolymer capsules.[21–23] However, for BCP capsules, the capsule formation process is much more complicated as microphase separation (between blocks) and macrophase separation (between HBNS and BCPs) occur simultaneously in the droplets. Crespy and co-workers recently reported the fabrication of BCP patchy capsules using hexadecane (HD) as the liquid cores.[24–26] However, the effect of polymer–solvent interactions on the capsule shell structure needs further exploration. Nowadays, it is still a great challenge to generate BCP capsules with tunable shell structures in a controlled fashion.

Although BCP capsules are robust enough for cargo loading and release, they are semipermeable and only allow for very small molecules to be loaded and released owing to the hydrophobic shell. To overcome this disadvantage, capsules with stimuli-responsive shells have been designed as smart nanocarriers to encapsulate functional species and release them in response to external triggers.[27–30] Furthermore, to tune the release behavior,[20,31–34] capsules with stimuli-responsive mesoporous shells are excellent candidates for controlling the release of payloads.[35–38] Remarkably, mass transfer through the capsule shell is strongly dependent on the shape, orientation, and uniformity of the pores.[39] Microphase separation of BCPs in the shell will provide great opportunities to generate ordered structures. However, it is still a challenge to obtain BCP capsules with precisely tunable pore structures in a convenient fashion. Moreover, the corresponding structure-dependent release behavior has not been well investigated.[25,28]

Herein, we describe the generation of BCP capsules with tunable shell structures by controlling the phase separation sequence through manipulation of the polymer–solvent interactions, and further illustrate their structure-dependent release behavior. Polystyrene-*block*-poly(4-vinylpyridine) (PS-*b*-P4VP) BCPs were employed to fabricate capsules with an HBNS liquid core (HD or perfluorooctane (PFO)) through the emulsion solvent evaporation strategy. The properties of the HBNS dictate the formation mechanism of the capsules and the resulting shell structures. On the basis of precise structural control, capsules with spherical, cylindrical, or lamellar mesopores were successfully obtained. Moreover, we further demonstrate the relationship between pore structure and release behavior. Interestingly, capsules with spherical pores displayed the best permeability with the fastest release process whereas those with lamellar pores showed the slowest, but stepwise, release. The drug-loaded capsules with different release behaviors were evaluated for inducing apoptosis in A375 melanoma cells, and different apoptosis ratios were indeed observed. We anticipate that these findings will be helpful for understanding the funda-

[*] Dr. J. Xu,[+] Y. Yang, Dr. K. Wang, Dr. J. Li, Dr. R. Liang, Prof. L. Shen, Prof. X. Xie, Prof. J. Zhu
Key Laboratory of Material Chemistry for Energy Conversion and Storage, Ministry of Education
School of Chemistry and Chemical Engineering
Huazhong University of Science and Technology (HUST)
Wuhan 430074 (China)
E-mail: jtzhu@mail.hust.edu.cn
Dr. J. Li,[+] N. Xu, Prof. J. Tao
Department of Dermatology, Union Hospital
Tongji Medical College, HUST
Wuhan 430022 (China)
E-mail: tjhappy@126.com
[+] These authors contributed equally to this work.

Supporting information for this article can be found under: http://dx.doi.org/10.1002/anie.201607982.

mental features of structured-capsule formation and that these capsules will be applied for the programmable release of active species.

The BCP capsules were prepared through the emulsion solvent evaporation route (see the Supporting Information for experimental details). Typically, the BCPs were dissolved in chloroform containing a small amount of HD (an HBNS for the copolymers) and then emulsified with an aqueous solution of poly(vinyl alcohol). The macrophase separation between the HD and BCP solutions takes place when the droplet composition reaches the binodal boundary during chloroform evaporation.[21,22] Through this route, PS-*b*-P4VP capsules with HD cores were fabricated. Surprisingly, the BCP molecular weight (19800–217000 Da), the block ratio (symmetric or asymmetric), and the chain architecture (AB diblock or ABA triblock) have no significant effect on the shell structure. Instead, only capsules with spherical P4VP domains in the shell (S-capsule) were observed (Figure 1; see also the Supporting Information, Figures S1 and S2).

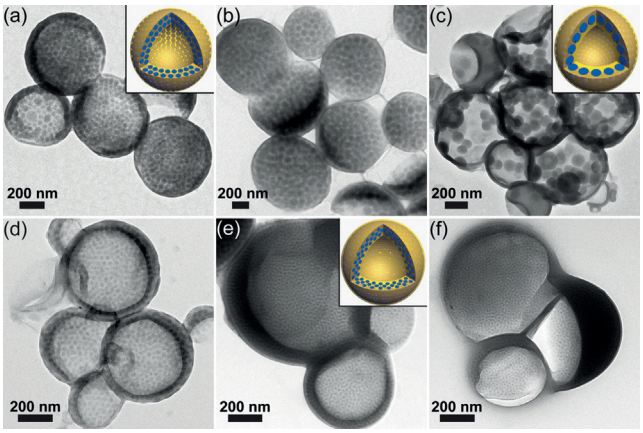

Figure 1. TEM images of BCP capsules obtained by employing HD as the liquid core: a) PS_{22K}-*b*-$P4VP_{22K}$, b) PS_{110K}-*b*-$P4VP_{107K}$, c) PS_{17K}-*b*-$P4VP_{49K}$, d) PS_{51K}-*b*-$P4VP_{18K}$, e) $P4VP_{4.5K}$-*b*-PS_{27K}-*b*-$P4VP_{4.5K}$, and f) $P4VP_{4.5K}$-*b*-PS_{38K}-*b*-$P4VP_{4.5K}$. The initial BCP/HD volume ratio was 4:6 for all samples. P4VP was stained with I_2 vapor before TEM analysis. The insets (a, c, and e) are cartoons showing the shell structures of the capsules. Blue and yellow regions represent P4VP and PS domains, respectively.

This unusual phenomenon was ascribed to the sequential nature of the process, that is, micellization of the BCPs and formation of the HD cores. We hypothesized that the order of the two types of phase separation would significantly affect the capsule structure. As the LBGS evaporates, the solubility of the BCPs will decrease owing to the increase in the HBNS fraction. Two possible pathways (Scheme 1) are expected when the fraction of HBNS reaches a critical value: I) The BCPs aggregate into micelles, and then the HBNS starts separating to direct the deposition of the micelles, or II) macrophase separation of HBNS occurs before the aggregation of the BCP chains, and then the BCPs migrate to the external oil/water interface to form the shell.[22]

To test the proposed mechanism, we performed a series of control experiments (Figures S3 and S4). As the chloroform evaporates, the mixed solution of PS-*b*-P4VP and HD

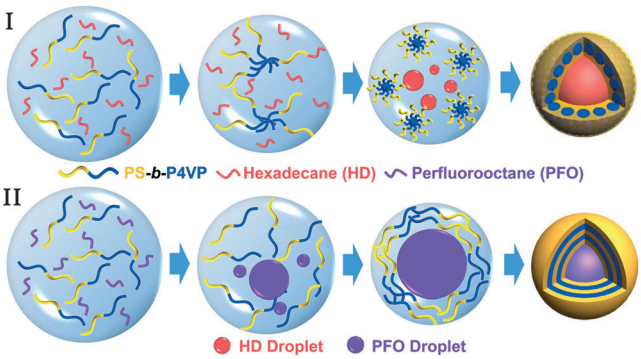

Scheme 1. The two possible pathways (I and II) for the formation of structured BCP capsules through the emulsion solvent evaporation method by introducing HD or PFO. Different shell structures can be obtained from the same BCP with different formation pathways.

becomes gradually cloudy from top to bottom, indicating the formation of BCP micellar aggregates (Figure S3). No HD droplets (i.e., no macrophase separation) could be observed owing to the good compatibility and solubility of HD (solubility parameter $\delta_{HD} = 16.4\ MPa^{1/2}$) and chloroform ($\delta_C = 19.0\ MPa^{1/2}$). A further increase in the relative amount of HD will induce micelle aggregation (Figure S4). Similarly, spherical micelles are formed before the macrophase separation of HD in the droplets upon evaporation of chloroform (Scheme 1 and Figure S5 a–e). As shown in Table S1 for the characteristics of solvents and polymers,[40] HD has a higher affinity to PS blocks ($\delta_{PS} = 18.6\ MPa^{1/2}$) than to P4VP ($\delta_{P4VP} = 22.2\ MPa^{1/2}$) blocks. The Flory–Huggins interaction parameters of these solvent–polymer pairs ($\chi_{S\text{-}P}$) were also calculated according to Equation (1),[40]

$$\chi_{S\text{-}P} = \frac{V_S(\delta_S - \delta_P)^2}{RT} + 0.34 \quad (1)$$

where V_S is the molar volume of the solvent, R refers to the ideal gas constant, and T is temperature. According to the Flory–Huggins criterion, complete solvent–polymer miscibility is expected when $\chi_{S\text{-}P} < 0.5$ whereas the solvent is poor for the polymer when $\chi_{S\text{-}P} > 0.5$. Here, the $\chi_{HD\text{-}PS}$ and $\chi_{HD\text{-}P4VP}$ values were determined to be 0.91 and 4.31, respectively. Thus, an increase in the fraction of HD results in the formation of spherical micelles with P4VP cores and PS coronas (Figure S4). This strategy also allowed us to tailor the shell thickness of the formed capsules by varying the volume fraction of HD (Figure S2). Moreover, to test the generality of this technique, we employed alkanes with various chain lengths to fabricate BCP capsules. Similarly, S-capsules were obtained when high-boiling alkanes were employed (Figure S6).

Considering the proposed formation mechanism, controlling the sequence of macrophase and microphase separation will give rise to BCP capsules with tunable shell structures. In general, macrophase separation only occurs at very high HD concentrations (Figure S5 a–e). Decreasing the affinity of alkanes to polymers and reducing the solubility of alkanes in chloroform are expected to induce macrophase separation of polymer and alkanes ahead of BCP aggregation.[41,42] Here,

PFO was selected as the HBNS. In this case, for symmetric $PS_{9.8K}$-*b*-$P4VP_{10K}$, capsules with lamellar shell structures (Figure 2a) were obtained instead of spherical shell structures (Figure S2e,f). According to Equation (1), the $\chi_{PFO\text{-}PS}$ and $\chi_{PFO\text{-}P4VP}$ values were 4.70 and 10.75, respectively, which are much larger than $\chi_{HD\text{-}PS}$ and $\chi_{HD\text{-}P4VP}$ (Table S1). PFO will segregate out at the early stage of the evaporation (Figure S3 and Figure S5 f–o). Therefore, the residual PFO in chloroform is not enough to induce the aggregation of BCP chains to micelles (Figure S3, where no turbidity can be observed), resulting in a shell with an undisturbed microphase-separated structure (Figure S7). In this case, the shell structures of the BCP capsules could be easily tailored by varying the block ratio of the BCPs. Asymmetric PS_{51K}-*b*-$P4VP_{18K}$ with a minor P4VP block (24.3 vol%) will form capsules with spherical P4VP domains (Figure 2b), agreeing well with its bulky phase structure. Furthermore, this technique is general and can be used to fabricate capsules from ABA (Figure 2c,d) or ABC (Figure S8) triblock copolymers. The shell thickness (34–164 nm) and the thickness/radius ratio (0.11–0.61) of the capsules can be tailored by simply adjusting the BCP/PFO feed ratio (Figures S9 and S10). The shape of the P4VP(PDP) domain does not undergo any obvious changes as the shell thickness is decreased, presumably because the confining effect exerted on the BCP chains is not strong enough. A further decrease of the shell thickness will result in the formation of broken capsules.

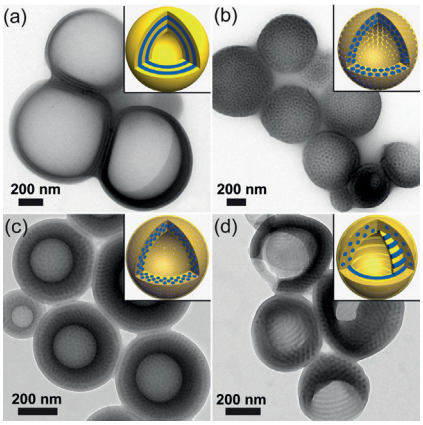

Figure 2. TEM images of the structured BCP capsules obtained by using PFO as the liquid core: a) $PS_{9.8K}$-*b*-$P4VP_{10K}$, b) PS_{51K}-*b*-$P4VP_{18K}$, c) $P4VP_{4.5K}$-*b*-PS_{38K}-*b*-$P4VP_{4.5K}$, and d) $P4VP_{4.5K}$-*b*-PS_{27K}-*b*-$P4VP_{4.5K}$.

In addition, an alternative strategy to tune shell structures is introduced that is based on employing BCP-based supramolecules without having to synthesize BCPs with various molecular weights and block ratios. The supramolecules consisted of PS-*b*-P4VP and 3-*n*-pentadecylphenol (PDP), which were connected through a hydrogen bond between the 4VP unit and PDP.[43–45] Yet, when HD was selected as the HBNS, PS-*b*-P4VP(PDP)$_x$ (x refers to the molar ratio of PDP to 4VP) capsules could not be obtained owing to the enhanced affinity between HD and PDP (Figure S11).[30] Fortunately, PS-*b*-P4VP(PDP)$_x$ capsules were observed when PFO was employed as PFO is immiscible with P4VP-(PDP). Taking $P4VP_{4.5K}$-*b*-PS_{38K}-*b*-$P4VP_{4.5K}(PDP)_x$ capsules as an example, the shell structure changes from a sphere ($x=0$, Figure 2c) to a cylinder ($x=0.25$), network ($x=0.5$), and then lamellae ($x=1.0$) as the PDP content is increased (Figure 3a–c). This approach can also be applied to the diblock copolymer PS_{51K}-*b*-$P4VP_{18K}(PDP)_x$, demonstrating the robustness of controlling shell structures by PDP addition (Figure S12).

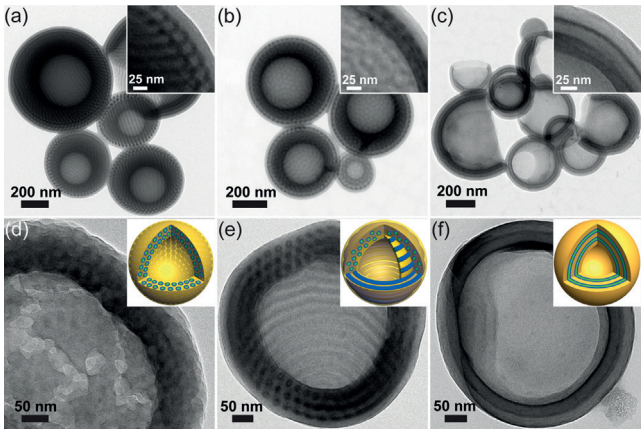

Figure 3. a–c) TEM images of $P4VP_{4.5K}$-*b*-PS_{38K}-*b*-$P4VP_{4.5K}(PDP)_x$ capsules, where x equals to a) 0.25, b) 0.50, and c) 1.0. d–f) TEM images and schematic illustrations of mesoporous $P4VP_{4.5K}$-*b*-PS_{38K}-*b*-$P4VP_{4.5K}$-$(PDP)_x$ capsules, where x equals to d) 0, e) 0.25, and f) 1.0. In the inset cartoons, blue, yellow, and green regions correspond to P4VP domains, PS domains, and mesopores, respectively.

Moreover, the shell structure can also be tuned by adding homopolystyrene (hPS) to BCPs. In the "wet brush" regime, the cylindrical P4VP domains will be transformed into spherical domains after adding 25 wt% $hPS_{2.8K}$ to $P4VP_{4.5K}$-*b*-PS_{27K}-*b*-$P4VP_{4.5K}$ (Figure S13a). However, in the "dry brush" regime, macrophase separation between hPS_{876K} and BCPs will take place, and the structure of the BCPs in the capsular shell is not significantly influenced. Thus capsules with patchy shells can be obtained (Figure S13b,c).

The shell structures of the capsules play a key role in determining the permeability and thus the release kinetics of the payloads. The P4VP(PDP) domains can be turned into mesopores by swelling in ethanol or acidic water (see the Supporting Information for experimental details). Three typical capsules with spherical (S), cylindrical (C), and lamellar (L) mesopores (Figure 3d–f) were selected for investigating the structure dependence of the release behavior. The shell thicknesses of the selected capsules were almost the same (103.1 ± 19.3 nm, 98.6 ± 15.4 nm, and 110.3 ± 10.6 nm, respectively; see Figure S10b). After removal of the PFO core (Figure S14), a hydrophilic Rhodamine 6G (R6G) dye was encapsulated. The loading amounts were almost the same (12.3 wt%, 12.5 wt%, and 12.5 wt%), as determined by UV/Vis measurements. At pH 7.4, the release kinetics of the three capsules were almost the same, with a maximum of about 30 wt% of the dye released; at pH 4.0, however, the release was clearly accelerated (Figure 4a). An acidic environment will trigger the ionization of P4VP,

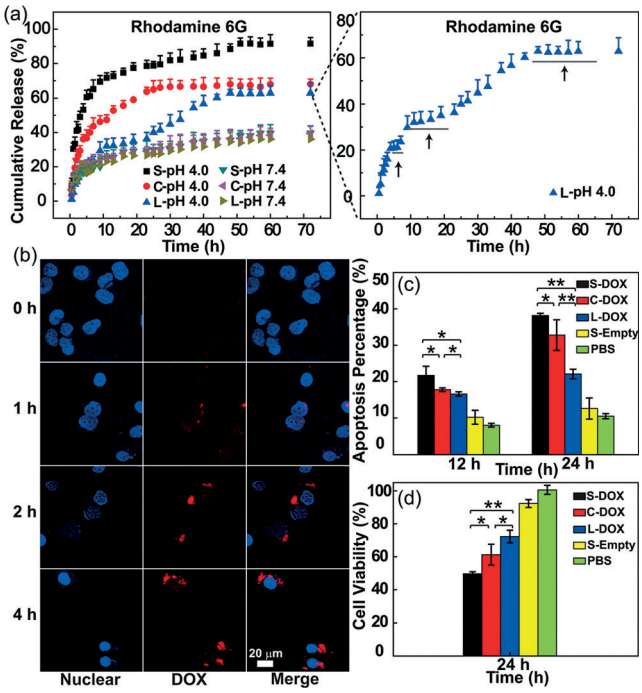

Figure 4. a) Left: Release profiles of R6G from capsules with different shell structures at different pH values. Right: The stepwise release profile of R6G from L-capsules at pH 4.0. Arrows indicate the three steps of the release process. b) Confocal laser scanning microscopy (CLSM) images of A375 cells treated with DOX-loaded S-capsules (DOX amount: 10 μg mL^{-1}). The scale bar in the last image can be applied to all other images. c) Analysis of the apoptosis of A375 cells induced by DOX-loaded capsules with different shell structures. The cells were incubated with the capsules for 12 or 24 h ($n=3$, Student's *t*-test, $*p<0.05$, $**p<0.01$). d) Cytotoxicity of the DOX-loaded capsules against A375 cells ($n=4$, Student's *t*-test, $*p<0.05$, $**p<0.01$). A375 cells treated with empty S-capsules (S-Empty) and PBS were used as the control groups.

facilitating the cargo release.[46] More interestingly, the release rates (R) of the capsules are in the order of $R_S > R_C > R_L$ at pH 4.0, indicating that the release kinetics are dominated by the shell structure.

The Baker–Lonsdale model [Eq. (2)],

$$\frac{3(1-(1-M_t/M_\infty)^{2/3})}{2} - M_t/M_\infty = \frac{3\,t\,D\,C_S}{r_0^2\,C_0} \qquad (2)$$

which is a classic model for the diffusion-controlled release from a spherical matrix, was used to model the release behavior of the capsules.[47,48] M_t and M_∞ are the released amounts at time t and infinite time, respectively; D, C_S, and C_0 are the diffusion coefficient, solubility, and initial concentration of payloads in the matrix, and r_0 is the radius of the capsule. As shown in Figure S15a and Table S2, the release of R6G at pH 7.4 can be excellently fitted to Equation (2) (coefficient of determination, $R^2 \geq 0.95$), indicating diffusion-controlled release in this case. The release rate constants ($k = 3\,D\,C_S/r_0^2\,C_0$) are 4.83×10^{-4} h^{-1} for the S-capsules at pH 7.4 (S-pH 7.4), 4.41×10^{-4} h^{-1} for C-pH 7.4, and 3.77×10^{-4} h^{-1} for L-pH 7.4 (Table S2). As r_0 is the same, and we further assumed C_S and C_0 to be the same (for steady release behavior), the D value is almost the same for all three types of capsules. This is reasonable as the capsule shells are solid at pH 7.4. On the other hand, the release behavior at pH 4.0 can be divided into several stages (Figure S15b,c), which can also be fitted by Equation (2). The D value of the first stage for S-pH 4.0 is 3.8 times larger than that for C-pH 4.0, 8.5 times larger than that for L-pH 4.0, and about 36.3 times larger than that for capsules at pH 7.4, respectively.[48] The results confirm the release rate order of $R_S > R_C > R_L$.

Considering the fact that the shell thicknesses are the same, we believe that the different release rates can be ascribed to the shape and distribution of the hydrophilic domains. First, the total surface area (A) of the hydrophilic domains dominates the D value of the cargoes across the capsule wall. The A values of the hydrophilic P4VP domains have been estimated to decrease in the order of $A_S > A_C > A_L$. Larger A values will facilitate cargo diffusion. Second, the hydrophobic PS matrix will retard the release. The space (i.e., the PS domain) between two adjacent P4VP microdomains (l) was determined to be 9.6 nm for spherical, 13.4 nm for cylindrical, and 19.5 nm for lamellar shell structures ($l_S < l_C < l_L$). Smaller distances increase the permeability of the capsule wall and increase the cargo release rate. Therefore, the release rate orders decrease according to $R_S > R_C > R_L$ at pH 4.0. More interestingly, the capsules with a lamellar structure displayed a stepwise release profile (Figure 4a). This was attributed to the concentric PS layers in the wall, which release the cargo in multiple steps.[28] A similar release profile was obtained upon using doxorubicin (DOX) instead of R6G in acid suspension (Figure S16), and the capsules remained unchanged after release (Figure S17).

The cellular uptake behavior and intracellular distribution of the DOX-loaded capsules were investigated in A375 melanoma cells. As shown in Figure 4b, the fluorescence intensity of DOX was significantly enhanced inside A375 cells after 4 h incubation, indicating efficient cellular uptake of the capsules. Flow cytometry analysis (Figure S18) was further carried out to evaluate the apoptosis ratios of A375 cells induced by DOX-loaded capsules with spherical (S-DOX), cylindrical (C-DOX), and lamellar (L-DOX) structures. After 12 h incubation, the apoptosis ratios of A375 cells induced by S-DOX, C-DOX, and L-DOX capsules (amount of DOX: 10 μg mL^{-1}) were 21.7%, 17.8%, and 16.6%, respectively. A similar trend was also observed when the incubation period was extended to 24 h, with apoptosis ratios of 38.2%, 32.8%, and 22.1%, respectively (Figure 4c). Moreover, the in vitro cytotoxicity of the loaded capsules for A375 cells was also evaluated. After incubation for 24 h, the cell viabilities were 49.7 ± 1.2%, 61.3 ± 6.3%, and 72.3 ± 3.8%, respectively (Figure 4d). The pH value within cancer cells gradually drops along the endocytic pathway from about 6.0–6.5 in endosomes to approximately 4.5–5.0 in lysosomes.[49] In the acidic environment, the P4VP domains in the capsules swell to yield mesopores with different shapes, leading to different DOX release profiles and different apoptosis ratios for cancer cells.

In summary, we have described two different formation pathways for BCP capsules and their structure-dependent release. It was found that the phase separation sequence

significantly affects the capsule shell structure. The properties of the HBNS have a great influence on the formation mechanism of the capsules and the phase separation sequence. The shell structures could be readily tailored by altering the block ratio, molecular weight, or using additives. These structured capsules can serve as excellent candidates for cargo storage and controlled release. Furthermore, we clearly confirmed the structure-dependent release behavior of BCP capsules with pH responsiveness. Capsules with spherical structures showed the best permeability with the fastest release process whereas those with lamellar structures showed the slowest, but stepwise, release profile. Different release behaviors further induce different apoptosis ratios in cancer cell studies. Our findings not only help to understand the fundamental mechanism of the capsule formation process, but also extend the application of structured BCP capsules as delivery vehicles with precise release kinetics. Future work will focus on tailoring the size and orientation of the mesopores in the capsule shells. In addition, the uniformity of the capsule size needs to be carefully considered as it may also affect the release behavior.

Acknowledgements

J.X. thanks Prof. Y. Y. Han (CIAC) and Prof. Y. G. Liao (HUST) for fruitful discussions. This work was funded by the NSFC (51525302 and 51473059) and the NSF of the Hubei Scientific Committee (2015BHE001). We also thank the HUST Analytical and Testing Center for allowing us to use its facilities.

Keywords: apoptosis · block copolymers · capsules · controlled release · phase separation

How to cite: *Angew. Chem. Int. Ed.* **2016**, *55*, 14633–14637
Angew. Chem. **2016**, *128*, 14853–14857

[1] K. Renggli, P. Baumann, K. Langowska, O. Onaca, N. Bruns, W. Meier, *Adv. Funct. Mater.* **2011**, *21*, 1241.
[2] A. Abbaspourrad, N. J. Carroll, S.-H. Kim, D. A. Weitz, *J. Am. Chem. Soc.* **2013**, *135*, 7744.
[3] B. M. Discher, Y. Y. Won, D. S. Ege, J. C. M. Lee, F. S. Bates, D. E. Discher, D. A. Hammer, *Science* **1999**, *284*, 1143.
[4] M. Urban, B. Freisinger, O. Ghazy, R. Staff, K. Landfester, D. Crespy, A. Musyanovych, *Macromolecules* **2014**, *47*, 7194.
[5] O. S. Kwon, J. Jang, J. Bae, *Curr. Org. Chem.* **2013**, *17*, 3.
[6] W. Meier, *Chem. Soc. Rev.* **2000**, *29*, 295.
[7] J. Cui, M. P. van Koeverden, M. Muellner, K. Kempe, F. Caruso, *Adv. Colloid Interface Sci.* **2014**, *207*, 14.
[8] J. W. Shim, S.-H. Kim, S.-J. Jeon, S.-M. Yang, G.-R. Yi, *Chem. Mater.* **2010**, *22*, 5593.
[9] X. Yu, Z. Zhao, W. Nie, R. Deng, S. Liu, R. Liang, J. Zhu, X. Ji, *Langmuir* **2011**, *27*, 10265.
[10] S.-H. Kim, H. C. Shum, J. W. Kim, J.-C. Cho, D. A. Weitz, *J. Am. Chem. Soc.* **2011**, *133*, 15165.
[11] A. Vimalanandan, L.-P. Lv, T. H. Tran, K. Landfester, D. Crespy, M. Rohwerder, *Adv. Mater.* **2013**, *25*, 6980.
[12] D. Crespy, M. Stark, C. Hoffmann-Richter, U. Ziener, K. Landfester, *Macromolecules* **2007**, *40*, 3122.
[13] W. Tong, X. Song, C. Gao, *Chem. Soc. Rev.* **2012**, *41*, 6103.
[14] M. K. M. Leung, G. K. Such, A. P. R. Johnston, D. P. Biswas, Z. Zhu, Y. Yan, J.-F. Lutz, F. Caruso, *Small* **2011**, *7*, 1075.
[15] K. Ariga, Y. M. Lvov, K. Kawakami, Q. Ji, J. P. Hill, *Adv. Drug Delivery Rev.* **2011**, *63*, 762.
[16] Y. Mai, A. Eisenberg, *Chem. Soc. Rev.* **2012**, *41*, 5969.
[17] L. Zhang, A. Eisenberg, *Science* **1995**, *268*, 1728.
[18] D. E. Discher, A. Eisenberg, *Science* **2002**, *297*, 967.
[19] W.-F. Dong, A. Kishimura, Y. Anraku, S. Chuanoi, K. Kataoka, *J. Am. Chem. Soc.* **2009**, *131*, 3804.
[20] H. Hu, G. Liu, *Macromolecules* **2014**, *47*, 5096.
[21] H. N. Yow, A. F. Routh, *Soft Matter* **2006**, *2*, 940.
[22] A. Loxley, B. Vincent, *J. Colloid Interface Sci.* **1998**, *208*, 49.
[23] E. Pisani, N. Tsapis, B. Galaz, M. Santin, R. Berti, N. Taulier, E. Kurtisovski, O. Lucidarme, M. Ourevitch, B. T. Doan, *Adv. Funct. Mater.* **2008**, *18*, 2963.
[24] R. H. Staff, M. Gallei, M. Mazurowski, M. Rehahn, R. Berger, K. Landfester, D. Crespy, *ACS Nano* **2012**, *6*, 9042.
[25] Y. Zhao, R. Berger, K. Landfester, D. Crespy, *Small* **2015**, *11*, 2995.
[26] R. H. Staff, P. Rupper, I. Lieberwirth, K. Landfester, D. Crespy, *Soft Matter* **2011**, *7*, 10219.
[27] W.-C. Yang, R. Xie, X.-Q. Pang, X.-J. Ju, L.-Y. Chu, *J. Membr. Sci.* **2008**, *321*, 324.
[28] M.-K. Park, S. Jun, I. Kim, S.-M. Jin, J.-G. Kim, T. J. Shin, E. Lee, *Adv. Funct. Mater.* **2015**, *25*, 4570.
[29] E. Amstad, S.-H. Kim, D. A. Weitz, *Angew. Chem. Int. Ed.* **2012**, *51*, 12499; *Angew. Chem.* **2012**, *124*, 12667.
[30] N. Paret, A. Trachsel, D. L. Berthier, A. Herrmann, *Angew. Chem. Int. Ed.* **2015**, *54*, 2275; *Angew. Chem.* **2015**, *127*, 2303.
[31] M. Motornov, Y. Roiter, I. Tokarev, S. Minko, *Prog. Polym. Sci.* **2010**, *35*, 174.
[32] S. Yu, T. Azzam, I. Rouiller, A. Eisenberg, *J. Am. Chem. Soc.* **2009**, *131*, 10557.
[33] L.-P. Lv, K. Landfester, D. Crespy, *Chem. Mater.* **2014**, *26*, 3351.
[34] H. C. Shum, J.-W. Kim, D. A. Weitz, *J. Am. Chem. Soc.* **2008**, *130*, 9543.
[35] P. F. Shi, Y. Q. Qu, C. G. Liu, H. Khan, P. C. Sun, W. Q. Zhang, *ACS Macro Lett.* **2016**, *5*, 88.
[36] J.-K. Kim, E. Lee, Y.-B. Lim, M. Lee, *Angew. Chem. Int. Ed.* **2008**, *47*, 4662–4666; *Angew. Chem.* **2008**, *120*, 4740–4744.
[37] R. H. Staff, M. Gallei, K. Landfester, D. Crespy, *Macromolecules* **2014**, *47*, 4876.
[38] X. Wang, G. Liu, J. Hu, G. Zhang, S. Liu, *Angew. Chem. Int. Ed.* **2014**, *53*, 3138; *Angew. Chem.* **2014**, *126*, 3202.
[39] I. Tokarev, S. Minko, *Adv. Mater.* **2010**, *22*, 3446.
[40] "Solubility Parameter Values": E. A. Grulke in *Polymer Handbook*, 4th ed. (Eds.: J. Brandrup, E. H. Immergut, E. A. Grulke), Wiley, New York, **1999**, Section VII, pp. 675–714.
[41] S. Torza, S. G. Mason, *Science* **1969**, *163*, 813–814.
[42] E. Pisani, N. Tsapis, J. Paris, V. Nicolas, L. Cattel, E. Fattal, *Langmuir* **2006**, *22*, 4397–4402.
[43] R. Deng, F. Liang, W. Li, S. Liu, R. Liang, M. Cai, Z. Yang, J. Zhu, *Small* **2013**, *9*, 4099–4103.
[44] R. Deng, S. Liu, J. Li, Y. Liao, J. Tao, J. Zhu, *Adv. Mater.* **2012**, *24*, 1889–1893.
[45] O. Ikkala, G. ten Brinke, *Science* **2002**, *295*, 2407–2409.
[46] Y. Wang, F. B. Li, *Adv. Mater.* **2011**, *23*, 2134–2148.
[47] "Controlled release: Mechanisms and rates": R. W. Baker, H. K. Lonsdale in *Controlled Release of Biologically Active Agents* (Eds.: A. C. Tanquary, R. E. Lacey), Plenum, New York, **1974**, pp. 15–71.
[48] S. Radin, T. Chen, P. Ducheyne, *Biomaterials* **2009**, *30*, 850–858.
[49] J. A. Mindell, *Annu. Rev. Physiol.* **2012**, *74*, 69–86.

Received: August 16, 2016
Revised: September 16, 2016
Published online: October 24, 2016

